Block Copolymer Templating Syntheses of Mesoporous Metal Oxides with Large Ordering Lengths and Semicrystalline Framework

Peidong Yang,[†] Dongyuan Zhao,[†,‡] David I. Margolese,[†]
Bradley F. Chmelka,[‡,§] and Galen D. Stucky*,[†,‡]

*Departments of Chemistry and Materials, Materials Research Laboratory, and Department of
Chemical Engineering, University of California, Santa Barbara, California 93106*

A simple and general procedure has been developed for the syntheses of ordered large-pore (up to 14 nm) mesoporous metal oxides, including TiO_2, ZrO_2, Nb_2O_5, Ta_2O_5, Al_2O_3, SiO_2, SnO_2, WO_3, HfO_2, and mixed oxides $SiAlO_y$, Al_2TiO_y, $ZrTiO_y$, $SiTiO_y$, ZrW_2O_y. Amphiphilic poly(alkylene oxide) block copolymers were used as structure-directing agents in nonaqueous solutions for organizing the network-forming metal oxide species. Inorganic salts, rather than alkoxides or organic metal complexes, were used as soluble and hydrolyzable precursors to the polymerized metal oxide framework. These thermally stable mesoporous oxides have robust inorganic frameworks and thick channel walls, within which high densities of nanocrystallites can be nucleated. These novel mesoporous metal oxides are believed to be formed through a mechanism that combines block copolymer self-assembly with alkylene oxide complexation of the inorganic metal species.

Introduction

Self-assembly of block copolymers,[1,2] surfactants,[3] colloidal suspensions[4] and proteins[5] provides a versatile approach to the creation of nanostructures with potential applications in biomaterials, optoelectronics, and nanotechnology.[6] Since the discovery of mesoporous silicates based on amphiphilic supramolecular templates,[7,8] the use of surfactant species to organize mesoporous silica has been explored over a wide range of conditions. Such conditions have relied on various interactions including electrostatic, hydrogen-bonding, covalent bonding, and van der Waals forces that have been balanced to achieve self-assembly and thereby direct mesostructure formation.[3,9–11] Recently, block copolymers have been increasingly used to organize mesostructured composite solids, because the architectures of the amphiphilic block copolymers can be rationally adjusted to control the interactions between the inorganic and organic species, self-assembly, and especially processibility more than possible with low molecular weight surfactants.[12] For example, using amphiphilic block copolymers as the structure-directing agents, aluminosilicate mesostructures,[13] and mesoporous silica[14–17] with large ordering lengths (>15 nm) and a variety of macroscopic morphologies (e.g., thin film and fiber) have been synthesized.

Extension of the surfactant templating procedure to the formation of non-silica mesoporous oxides, however, has been less widespread, although these mesoporous metal oxides hold more promise in applications that involve electron transport and transfer or magnetic interactions.[18] Mesoporous MnO_2,[19] Al_2O_3,[20,21] TiO_2,[22,23] Nb_2O_5,[11] Ta_2O_5,[11] ZrO_2,[24–28] HfO_2,[29] and SnO_2[30] and

* To whom correspondence should be addressed.
† Departments of Chemistry and Materials.
‡ Materials Research Laboratory.
§ Department of Chemical Engineering.
(1) Muthukumar, M.; Ober, C. K.; Thomas, E. L. *Science* **1997,** *277,* 1225.
(2) Fredrickson, G. H.; Bates, F. S. *Annu. Rev. Mater. Sci.* **1996,** *26,* 501.
(3) Huo, Q.; Margolese, D. I.; Ciesla, U.; Feng, P.; Gier, T. E.; Sieger, P.; Leon, R.; Petroff, P. M.; Schüth, F.; Stucky, G. D. *Nature* **1994,** *368,* 317.
(4) Van Blaaderen, A.; Ruel, R.; Wiltzius, P. *Nature* **1997,** *385,* 321.
(5) Ghadiri, M. R.; Cranja, J. R.; Buehler, L. K. *Nature* **1997,** *369,* 301.
(6) Yang P.; Deng T.; Zhao D.; Feng P.; Pine D.; Chmelka B. F.; Whitesides G. W.; Stucky G. D. *Science* **1998,** *282,* 2244.
(7) Kresge, C. T.; Leonowicz, M. E.; Roth, W. J.; Vartuli, J. C.; Beck, J. S. *Nature* **1992,** *359,* 710.
(8) Inagaki S.; Fukushima Y.; Kuroda K. *J. Chem. Soc., Chem. Commun.* **1993,** *8,* 680.
(9) Huo, Q.; Margolese, D. I.; Ciesla, U.; Demuth, D. G.; Feng, P.; Gier, T. E.; Sieger, P.; Firouzi, A.; Chmelka, B. F.; Schüth, F.; Stucky, G. D. *Chem. Mater.* **1994,** *6,* 1176.
(10) Tanev, P. T.; Pinnavaia, T. J. *Science* **1995,** *267,* 865.
(11) Antonelli, D. M.; Ying, J. Y. *Chem. Mater.* **1996,** *8,* 874.

(12) Förster, S.; Antonietti, M *Adv. Mater.* **1998,** *10,* 195.
(13) Templin, M.; Franck, A.; Chesne, A. D.; Leist, H.; Zhang, Y.; Ulrich, R.; Schädler, V.; Wiesner, U. *Science* **1997,** *278,* 1795.
(14) Zhao, D.; Feng, J.; Huo, Q.; Melosh, N.; Fredrickson, G. H.; Chmelka, B. F.; Stucky, G. D *Science* **1998,** *279,* 548.
(15) Zhao, D.; Yang, P.; Melosh, N.; Feng, J.; Chmelka, B. F.; Stucky, G. D. *Adv. Mater.* **1998,** *10,* 1380.
(16) Yang, P.; Zhao, D.; Chmelka, B. F.; Stucky, G. D. *Chem. Mater.* **1998,** *10,* 2033.
(17) Kramer E.; Forster S.; Goltner C.; Antonietti M. *Langmuir* **1998,** *14,* 2027.
(18) Sayari, A.; Liu, P. *Microporous Mater.* **1997,** *12,* 149.
(19) Tian, Z.; Tong, W.; Wang, J.; Duan, N.; Krishnan, V. V.; Suib, S. L. *Science* **1997,** *276,* 926.
(20) Bagshaw, S. A.; Pinnavaia, T. J. *Angew. Chem., Int. Ed. Engl.* **1996,** *35,* 1102.
(21) Vaudry F.; Khodabandeh S.; Davis M. E. *Chem. Mater.* **1996,** *8,* 1451.
(22) Antonelli, D. M.; Ying, J. Y. *Angew. Chem., Int. Ed. Engl.* **1995,** *34,* 2014.

reduced Pt[31] have been synthesized using low molecular weight surfactants over the past few years, although often thermally unstable mesostructures have resulted.[3,32,33] Stucky and co-workers developed a surfactant templating strategy for the synthesis of non-silica-based mesostructures, mainly metal oxides,[3,9] in which both positively and negatively charged low molecular weight surfactants were used in the presence of water soluble inorganic species. It was found that charge density matching between the surfactant and the inorganic species is important for the formation of the organic−inorganic mesophases. Unfortunately, many of these non-silica mesostructures are not thermally stable.

Pinnavaia and co-workers used nonionic surfactants to synthesize mesoporous alumina in neutral media and suggested that the resulting mesoporous materials with wormlike channels are assembled by hydrogen-bonding interactions of the inorganic species with the surfactant agents.[20] Antonelli and Ying prepared the stable mesoporous transition metal oxide, TiO_2, using a modified sol−gel method, in which an organometallic precursor was hydrolyzed in the presence of alkyl phosphate surfactants.[22] Mesoporous ZrO_2 was prepared using long-chain quaternary ammonium, primary amines, or amphoteric cocamidopropyl betaine as structure-directing agents.[26,27] A scaffolding process was developed by Knowles et al. for the preparation of mesoporous ZrO_2.[25] Porous HfO_2 has been synthesized using cetyltrimethyllammonium bromine as the structure-directing agent.[29] Suib et al. prepared mixed-valent semiconducting mesoporous maganese oxide with hexagonal and cubic structures and showed that these materials are catalytically active.[19] A ligand-assisted templating approach has been successfully used by Ying and co-workers for the synthesis of mesoporous Nb_2O_5 and Ta_2O_5.[11,22] Dative coordinate bond interactions between the inorganic and surfactant species were utilized in this process to assemble the mesostructure. Recently, Attard et al. have extended the surfactant templating strategy to produce mesoscopically ordered porous reduced platinum metal.[31] For all of these mesoporous non-silica materials, low molecular weight surfactants were used for the assembly of the mesostructures and the resulting mesoporous materials generally have small pore sizes (<4 nm). The channel walls of these mesoporous metal oxides have been exclusively amorphous. Most of the above syntheses were carried out in aqueous solution using metal alkoxides as inorganic precursors. The existence of a large amount of water makes the hydrolysis and condensation of the reactive metal alkoxides and the subsequent mesostructure assembly process difficult

to control. Little work has been done on mesostructure self-assembly in nonaqueous media using inorganic precursors.

We have developed a simple and general procedure for the synthesis of ordered large-pore (up to 14 nm) mesoporous metal oxides,[34] including TiO_2, ZrO_2, Nb_2O_5, Ta_2O_5, Al_2O_3, SnO_2, WO_3, HfO_2, and mixed oxides $SiAlO_y$, Al_2TiO_y, $ZrTiO_y$, $SiTiO_y$, and ZrW_2O_y. Amphiphilic poly(alkylene oxide) block copolymers are used as structure-directing agents in nonaqueous solutions for organizing network-forming metal species. Inorganic salts rather than alkoxides or organic metal complexes are used as precursors. These thermally stable mesoporous oxides have robust inorganic frameworks and thick channel walls, within which a high density of nanocrystallites can be nucleated and grown. These mesoporous metal oxides, therefore, can be produced with semicrystalline channel walls, which are expected to provide new opportunities for modifying their properties. The metal oxide−block copolymer composites are believed to form through the assembly of block copolymer species with the inorganic metal species complexing with the hydrophilic copolymer moiety. Since this complexation strategy relies on the unsaturated coordination spheres of the metal ions in the inorganic precursors, it can be applied to many different metal oxide systems quite generally.

Experimental Section

Chemicals. The block copolymer surfactants are commercially available from Aldrich, BASF, and Dow Chemical, and were used as received. Anhydrous metal chlorides are purchased from Alfa AEsar and Aldrich. Block copolymers include $HO(CH_2CH_2O)_{20}(CH_2CH(CH_3)O)_{70}(CH_2CH_2O)_{20}H$ (designated $EO_{20}PO_{70}EO_{20}$, BASF, Pluronic P-123), $HO(CH_2CH_2O)_{106}(CH_2CH(CH_3)O)_{70}(CH_2CH_2O)_{106}H$ (designated $EO_{106}PO_{70}EO_{106}$, BASF, Pluronic F-127), and $HO(CH_2CH_2O)_{75}(CH_2CH(CH_3CH_2)O)_{45}$ (designated $EO_{75}BO_{45}$, Dow Chemical).

Syntheses. In a typical synthesis, 1 g of poly(alkylene oxide) block copolymer was dissolved in 10 g of ethanol (EtOH) (for Hf system, butanol was used instead). To this solution, 0.01 mole of the respective anhydrous inorganic chloride precursor (Table 1) was added with vigorous stirring. (*Caution should be taken as most of these inorganic chlorides react violently with alcohol.*) The resulting sol solution was gelled in an open Petri dish at 40−60 °C in air. The aging times differed for the different inorganic systems and are listed in Table 1. Alternatively, the sol solution can be used to prepare thin films by dip coating. The thin films can be dried within several hours at 30−60 °C. The as-made bulk samples or thin films were then calcined at 300−600 °C for 4−5 h to remove the block copolymer surfactant species.

Characterization. Low-angle and wide-angle X-ray powder diffraction (XRD) patterns were obtained on a Scintag PADX diffractometer using Cu Kα radiation. To facilitate the beam-sample alignment during the low-angle (0.2−5°) XRD measurement on the as-made samples, the samples were prepared as follows: 1−2 drops of the sol solution were applied and uniformly distributed on a glass slide and then dried, as described above. Transmission electron microscopy (TEM) studies were carried out on a JEOL 2000 electron microscope operating at 200 keV. The samples for TEM were prepared by directly dispersing the fine powders of the products onto holey carbon copper grids. Energy-dispersive X-ray (EDX) spectra were taken on a Gatan detector connected to the electron microscope (electron beam size 10−100 nm). The

(23) Putnam R. L.; Nakagawa N.; McGrath K. M.; Yao N.; Aksay I. A.; Gruner S. M.; Navrotsky A. *Chem. Mater.* **1997**, *9*, 2690.

(24) Ciesla, U.; Schacht, S.; Stucky, G. D.; Unger, K. K.; Schüth, F. *Angew. Chem., Int. Ed. Engl.* **1996**, *35*, 541.

(25) Knowles J. A.; Hudson M. J. *Chem. Commun.* **1995**, 2083.

(26) Kim, A.; Bruinsma P.; Chen Y.; Wang L.; Liu J. *Chem Commun.* **1997**, 161.

(27) Pacheco G.; Zhao E.; Garcia A.; Sklyarov A.; Fripiat J. J. *Chem Commun.* **1997**, 491.

(28) Wong M. S.; Ying J. Y. *Chem. Mater.* **1998**, *10*, 2067.

(29) Liu, P.; Liu, J.; Sayari, A. *Chem. Commun.* **1997**, 557.

(30) Severin, K. G.; AbdelFattah, T. M.; Pinnavaia, T. J. *Chem. Commun.* **1998**, 1471.

(31) Attard, G. S.; Barlett P. N.; Coleman N. R. B.; Elliott J. M.; Owen, J. R.; Wang, J. H. *Science* **1997**, *278*, 838.

(32) Ulagappan, N.; Rao, C. N. R. *Chem. Commun.* **1996**, 1685.

(33) Braun, P. V.; Osenar, P.; Stupp, S. I. *Nature* **1996**, *380*, 325.

(34) Yang, P.; Zhao, D.; Margolese, D. I.; Chmelka, B. F.; Stucky, G. D. *Nature* **1998**, *396*, 512.

Table 1. Syntheses Conditions (Precursor, Temperature, Aging Time) and the Ordering Lengths for the As-Synthesized Mesostructures

system	inorganic precursor	aging temp (°C)	aging time (day)	d (Å)
Zr	$ZrCl_4$	40	1	115
Ti	$TiCl_4$	40	7	123
Sn	$SnCl_4$	40	2	124
Nb	$NbCl_5$	40	2	106
Ta	$TaCl_5$	40	2	110
W	WCl_6	60	15	126
Hf	$HfCl_4$	40	1	124
Ge	$GeCl_4$	40	15	146
V	VCl_4	60	7	111
Zn	$ZnCl_2$	60	30	120
Cd	$CdCl_2$	40	7	111
In	$InCl_3$	60	30	124
Sb	$SbCl_5$	60	30	93
Mo	$MoCl_5$	60	7	100
Re	$ReCl_5$	60	7	121
Ru	$RuCl_3$	40	3	95
Ni	$NiCl_2$	40	2	100
Fe	$FeCl_3$	40	7	116
Cr	$CrCl_3$	40	4	117
Mn	$MnCl_2$	40	7	124
Cu	$CuCl_2$	40	7	98
SiAl	$AlCl_3/SiCl_4$	40	2	120
Si_2Al	$AlCl_3/SiCl_4$	40	2	130
ZrTi	$ZrCl_4/TiCl_4$	40	2	110
Al_2Ti	$AlCl_3/TiCl_4$	40	7	112
SiTi	$SiCl_4/TiCl_4$	40	3	103
ZrW_2	$ZrCl_4/WCl_6$	40	3	140
SnIn	$SnCl_4/InCl_3$	40	30	83

nitrogen adsorption and desorption isotherms at 77 K were measured using a Micromeritics ASAP 2000 system after the samples were vacuum-dried at 200 °C overnight. The sorption data were analyzed using the Barrett–Joyner–Halenda (BJH) model with Halsey equation[35] and with the Broekoff–de Boer (BdB) model.[36] For the BJH analysis, the pore size distribution was obtained from the analysis of the adsorption branch of the isotherm. In the BdB analysis, both the adsorption and desorption branches were used to calculate the pore size distribution. The pore volume was taken at the $P/P_0 = 0.983$ signal point. Solid-state ^{27}Al and ^{29}Si MAS NMR spectra were recorded on a General Electric GN-300 spectrometer. A Netzsch thermoanalyzer STA 409 was used for simultaneous thermal analysis combining thermogravimetry (TG), derivative thermogravimetry(DTG), and differential thermoanalysis (DTA) with a heating rate of 5 K min^{-1} in air. A Sony optical microscope was used to study the polarization behavior and surface textures of the samples.

Results and Discussion

Table 1 summarizes the synthetic conditions and results for as-made inorganic/block copolymer meso-structured composites using $EO_{20}PO_{70}EO_{20}$ as the structure-directing agent. Most of the inorganic chlorides react with the alcohol solvent and form monolithic mesostructured gel composites. A broad range of the mesostructured composites have been prepared, including the first-, second-, and third-row transition metals and some main group elements as well. Most of the products form hexagonal mesophases, while lamellar and cubic mesophases are also observed for certain systems. The ordering lengths shown in the table correspond to the largest d value observed from the low-angle XRD patterns of these mesostructured composites.

(35) Gregg, S. J.; Sing, K. S. W. *Adsorption, surface area and porosity*; Academic Press: London, 1982.
(36) Broekhoff, J. C. P.; deBoer, J. H. *J. Catal.* **1967**, *9*, 8.

They range from 70 to 170 Å for the different systems. High order low-angle diffraction peaks are also observed for many of these systems. Quantitative elemental analyses suggest that the walls of these mesostructured composites are made up of metal–oxygen–chlorine networks. This is consistent with the fact that many of these metal chlorides (e.g., Ti, Zr, Sn, Al, Si, Nb, Ta, V, Mo, W, etc.) can react vigorously with alcohol to form $M(OR)_xCl_{n-x}$ ($n = 4-6$, $x = 1-3$), and these $M(OR)_xCl_{n-x}$ species then undergo cross-linking process to form the inorganic frameworks of the resultant composite meso-structures. Upon calcination, mesoporous TiO_2, ZrO_2, Nb_2O_5, Ta_2O_5, SnO_2, Al_2O_3, WO_3, and HfO_2 and $Si_{1-x}Al_xO_y$, $SiTiO_y$, Al_2TiO_y, $ZrTiO_y$, and ZrW_2O_y are obtained while other (M = Ge, V, Zn, Cd, In, Sb, Mo, Re, Ru, Ni, Fe, Cr, Mn, Cu, etc.) mesoscopically ordered composites prepared under the above conditions did not maintain the mesoscopic ordering following calcination.

The success of obtaining a specific mesoporous metal oxide depends on two factors: (1) the occurrence of a three-dimensional mesophase and (2) the stability of the inorganic framework upon removal of the surfactant species. Hexagonal and cubic mesophases are preferred when $EO_{20}PO_{70}EO_{20}$ and $EO_{106}PO_{70}EO_{106}/EO_{75}BO_{45}$ are used as the structure-directing agents, respectively. The stability of a mesostructure depends on the extent of the condensation and crystallinity of the inorganic walls. A higher degree of polymerization tend to impart improved thermal stability. The polymerization of the inorganic species is normally achieved by adjusting the pH and the reaction temperature. Furthermore, the interaction between the surfactant and inorganic wall should not be too strong, so that the mesostructure assembly can take place and the surfactant can be easily removed without damage to the integrity of the channel walls. For this purpose, hydrogen bonding, and/or weak coordination bonds are more preferred than electrostatic interactions and covalent bonding. In addition, the redox chemistry of the various transition metals can also affect the thermal stability of the resultant mesoporous metal oxides.[19]

This study used nonionic amphiphilic block copolymers as the structure-directing agents. These block copolymers promote the cooperative assembly of inorganic/copolymer mesostructures with relatively weak interactions at the inorganic/organic interface, yielding mesostructured thermally stable metal oxides. In the following sections, we will present the detailed characterization results for each of these mesoporous metal oxides prepared in this study.

Titania. Figure 1 shows typical XRD patterns for mesostructured titanium oxides, prepared using $EO_{20}PO_{70}EO_{20}$ as the structure-directing agent, before and after calcination. The as-synthesized titanium inorganic/polymer mesostructure (Figure 1a) shows three diffraction peaks with $d = 123$, 73, and 63 Å. After calcination, the diffraction peaks appear at higher 2θ angles with $d = 101$, 53 Å (Figure 1b). Both sets of diffraction peaks can be indexed as the (100), (110), and/or (200) reflections from two-dimensional (2D) hexagonal mesostructures with lattice constants $a_0 = 142$ and 117 Å, respectively.

When $EO_{75}BO_{45}$ is used as the structure-directing agent, a cubic mesophase of TiO_2 was obtained. The
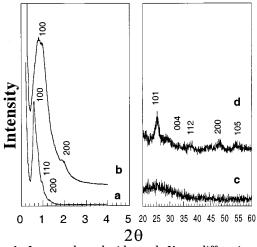
Figure 1. Low-angle and wide-angle X-ray diffraction (XRD) patterns of (a and c) as-synthesized $Ti(O,Cl)/EO_{20}PO_{70}EO_{20}$ composite mesostructure and (b and d) calcined mesoporous TiO_2.

as-made titanium inorganic/polymer mesostructure shows six diffraction peaks with $d = 100, 70, 58, 44, 41$, and 25 Å (d value ratio $\sqrt{2}:\sqrt{4}:\sqrt{6}:\sqrt{10}:\sqrt{12}:\sqrt{32}$), which can be indexed as (110), (200), (211), (310), (222), (440) reflections of a $Im3m$ mesophase with lattice constant $a_0 = 141$.[34] After calcination, the diffraction peaks appear at higher 2θ angles with $d = 76, 53$, and 43 Å. These diffraction peaks can be indexed as the (110), (200), and (211) reflections from $Im3m$ mesostructure with lattice constant 107 Å.

Thermogravimetric experiments indicate that the block copolymers are completely removed upon calcination in air at 400 °C. The appearance of low-angle diffraction peaks (Figs. 1b) indicates that mesoscopic order is preserved in the calcined TiO_2 materials. This is confirmed by TEM studies. For example, parts a and b of Figure 2 show TEM images of mesoporous TiO_2 recorded along and normal to the channel axis of the two-dimensional hexagonal mesostructures. Figure 2c shows a TEM image of the cubic TiO_2 mesophase prepared using $EO_{75}BO_{45}$ as the structure-directing agent. A square lattice of the pores can be clearly seen in this image. The pore/channel walls are continuous and have a thickness of ~5 nm. In addition, EDX measurements made on the calcined samples show signals only from Ti and Cu (from the copper grids) (Figure 2c inset), which confirms that the inorganic wall materials consist of essentially metal–oxygen networks. It is also found that for as-made samples the Ti:Cl molar ratio is 1:1.5, although there is no detectable Cl after the calcination from quantitative elemental analysis. This indicates that Cl is not incorporated into the calcined inorganic framework, consistent with the results obtained from EDX and thermogravimetric analyses on the as-made samples.

Selected area electron diffraction patterns recorded on mesoporous TiO_2 show that the walls of these materials are comprised of nanocrystalline oxides that show characteristic diffuse electron diffraction rings (Figure 2a inset). Wide-angle X-ray diffraction studies of calcined samples also clearly show broad peaks that can be indexed according to the anatase crystalline phase. Figure 1d shows wide-angle diffraction patterns for the calcined TiO_2 sample. The sizes of the nano-
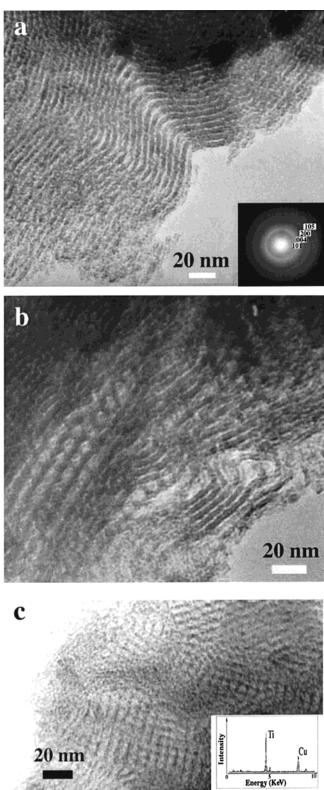

Figure 2. TEM micrographs of two-dimensional hexagonal mesoporous TiO_2 recorded along the (a) [ll0] and (b) [001] zone axes, respectively. Inset in part a is selected-area electron diffraction patterns obtained on the image area. (c) TEM image of cubic mesoporous TiO_2 accompanied by the corresponding (inset) EDX spectrum acquired for this sample.

crystals in the calcined materials are estimated to be ~3 nm by applying the Scherrer formula on the (101) diffraction peak. Furthermore, bright-field and dark-field TEM imaging were employed to study the distribution of these nanocrystals within the mesoporous TiO_2.
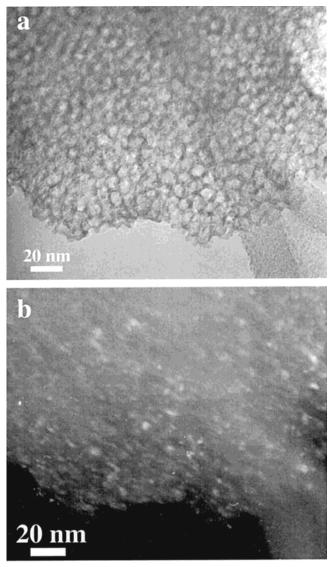
Figure 3. (a) Bright-field TEM image of a thin slice of the hexagonal mesoporous TiO_2 sample. (b) Dark-field image obtained on the same area of the same TiO_2 sample. The bright spots in the image correspond to TiO_2 nanocrystallites.

Parts a and b of Figure 3 show such images recorded on same area of one thin mesoporous TiO_2 sample. As can be seen in the dark field image (Figure 3b), the TiO_2 nanocrystals (~3 nm) are distributed across the sample. Reconciling the contrast features in Figure 3a,b indicates that the nanocrystals are embedded in the continuous amorphous titania matrix to form semicrystalline wall structures.

Nanocrystallite intergrowth during the calcination process thus yields mesoporous products with semicrystalline inorganic channel walls. Large hysteresis loops that resemble typical H_1- and H_2- type N_2 adsorption/desorption isotherms are observed for these materials. For example, Figure 4 shows nitrogen sorption isotherms that are representative of mesoporous cubic TiO_2. Such strong hysteresis is believed to be related to the capillary condensation associated with large pore channels and/or cages. Barrett–Joyner–Halenda (BJH) analyses show that the calcined hexagonal and cubic mesoporous TiO_2 exhibit mean pore sizes of 65 and 68 Å (Figure 4 inset), respectively with surface area of 200 m^2/g and porosity of 50%.[37] BdB analyses yield similar
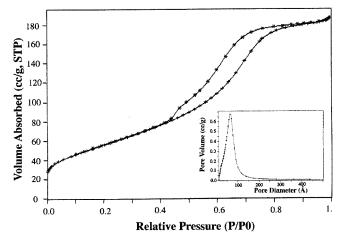

Figure 4. Nitrogen adsorption–desorption isotherms and BJH pore-size distribution plot (inset) for calcined cubic mesoporous TiO_2.

mean pore sizes for these materials.[38] To the best of our knowledge, such pore sizes are the largest reported for mesoporous titania. Their surface areas are lower than those reported by Ying et al. for TiO_2 prepared using low molecular weight surfactants having smaller pore sizes.[22] These results are reasonable considering the larger pore size in our mesoporous titania, and that for equivalent porosities, surface area is inversely proportional to the pore size.

Due to its low cost, ease of handling, and high resistance to photoinduced corrosion, titanium oxide is one of the most studied semiconductors for the photocatalytic reactions.[39] The effectiveness of titania as a photocatalyst depends on its crystal phase, particle size, and crystallinity. Among the common crystalline forms of titania, anatase is generally recognized to be the most active photocatalyst phase. It was recently demonstrated, however, that mesoporous titania prepared using ligand-assisted templating methods has low photocatalytic activity compared to the crystalline phase despite their high surface area.[40] Because the phosphate surfactants used in those studies strongly bonded to the titania framework, they cannot be removed completely either by calcination or solvent extraction. This, combined with the amorphous titania channel walls, affords low quantum yield for the photocatalytic reactions. The results lead the authors to conclude that partially crystallized titania is essential for obtaining high photocatalytic activity. Although our samples have surface areas lower than those prepared through ligand-assisted templating approach, the semicrystalline channel walls are expected to afford higher overall activity toward photocatalysis reactions.

Zirconia. The as-made zirconium inorganic/polymer mesostructure shows three diffraction peaks with $d =$ 115, 65, and 59 Å.[34] After calcination, the diffraction peaks appear at higher 2θ angles with $d =$ 106, 60, and

(37) Calcination at above 600 °C resulted in extensive crystal growth of anatase, consequently, the mesostructures collapsed and the surface area was significantly reduced to 30 m^2/g.

(38) For example, BdB analysis of hexagonal mesoporous TiO_2 using cylindrical pore model gives pore size of 65 Å from both the adsorption and desorption isotherms.

(39) Zhang, Z. B.; Wang, C. C.; Zakaria, R.; Ying, J. Y. *J. Phys. Chem. B* **1998**, *102*, 10871.

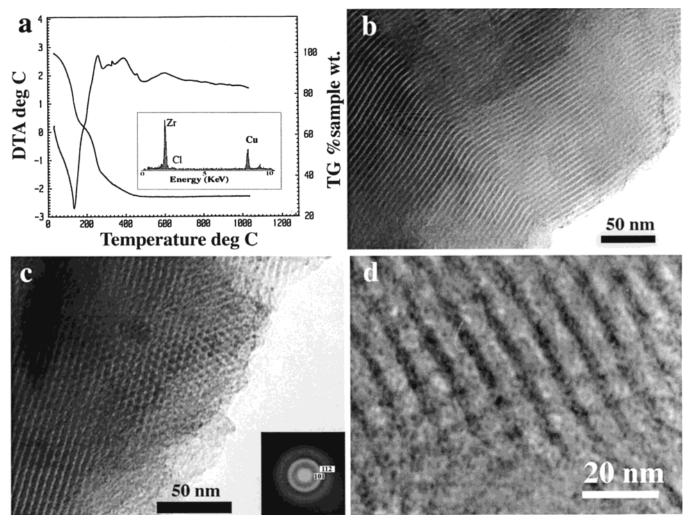(40) Stone, V. F.; Davis, R. J. *Chem. Mater.* **1998**, *10*, 1468.

Figure 5. (a) TGA trace recorded for the as-synthesized Zr(O,Cl)/EO$_{20}$PO$_{70}$EO$_{20}$ composites. (b and c) TEM micrographs of two-dimensional hexagonal mesoporous ZrO$_2$ recorded along the [ll0] and [001] zone axes, respectively. Inset in part c is selected-area electron diffraction pattern obtained on the image area. (d) TEM image of cubic mesoporous ZrO$_2$.

53 Å. Both sets of diffraction peaks can be indexed as the (100), (110), and (200) reflections associated with two-dimensional hexagonal mesostructures with lattice constants $a_0 = 132$ and 122 Å, respectively.

Thermogravimetric experiments indicate that the block copolymers are completely removed from the as-synthesized zirconium composites upon calcination at 400 °C (Figure 5a). The appearance of low-angle diffraction peaks indicates that mesoscopic order is preserved in the calcined ZrO$_2$ materials, as confirmed also by TEM images. For example, parts b and c of Figure 5 show TEM images of mesoporous ZrO$_2$ recorded along the [ll0] and [001] zone axes of the two-dimensional hexagonal mesostructures. In each case, mesoscopically ordered large channels are clearly observed to be arranged in hexagonal arrays. When EO$_{75}$BO$_{45}$ is used as the structure-directing agent, a cubic mesophase of ZrO$_2$ was obtained, a TEM of which is shown in Figure 5d. The pore/channel walls are continuous and have thicknesses ~6.5 nm. In addition, EDX measurements made on the calcined samples show the expected primary metal element signals, with only a trace of Cl (Figure 5a inset), which confirms that the inorganic wall materials consist of predominantly metal−oxygen networks. This is consistent with thermogravimetric analyses performed on the as-made samples and the quan-

titative elemental analyses of the as-made and calcined zirconia samples. For the as-made samples, Zr:Cl molar ratio is 1:1.6, while only 0.4% (wt) of Cl was detected in the calcined samples.

Selected-area electron diffraction patterns recorded on mesoporous ZrO$_2$ show that the walls of these materials are made up of nanocrystalline oxides that show characteristic diffuse electron diffraction rings (Figure 5c inset). Wide-angle X-ray diffraction studies of calcined samples clearly show broad peaks that can be indexed according to the tetragonal phase of crystalline ZrO$_2$.[34] The sizes of the nanocrystallites in the calcined materials are estimated to be ~2 nm by applying the Scherrer formula on the (101) diffraction peak. Furthermore, bright-field and dark-field TEM imaging were employed to study the distribution of these nanocrystals. Parts a and b of Figure 6 show such images recorded from the same area of one thin mesoporous ZrO$_2$ sample. Reconciling the contrast in these images indicates the ZrO$_2$ nanocrystallites (~2 nm) are embedded in the mesoscopically ordered but otherwise amorphous matrix to form semicrystalline wall structures.

BJH analyses of nitrogen sorption isotherms show that the calcined hexagonal and cubic mesoporous ZrO$_2$ exhibit pore sizes of 58 and 62 Å, respectively.[41] Large

Block Copolymer Templating Syntheses

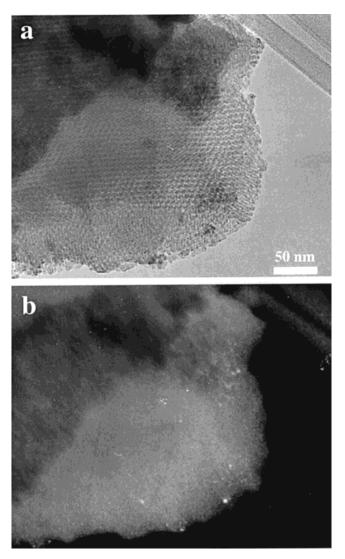*Chem. Mater., Vol. 11, No. 10, 1999* **2819**

Figure 6. (a) Bright-field TEM image of a thin slice of the hexagonal mesoporous ZrO_2 sample. (b) Dark-field image obtained on the same area of the same ZrO_2 sample. The bright spots in the image correspond to ZrO_2 nanocrystallites.

Figure 7. Low-angle and wide-angle X-ray diffraction (XRD) patterns of (a and c) as-synthesized $Nb(O,Cl)/EO_{20}PO_{70}EO_{20}$ composite mesostructure and (b and d) calcined mesoporous Nb_2O_5.

hysteresis loops that resemble typical H_1- and H_2-type isotherms are also observed for these mesoporous ZrO_2 samples. These mesoporous zicornia samples have surface areas of 150 m^2/g and porosities of ~45%. There has previously been substantial work on the preparation of mesoporous ZrO_2 using low molecular weight surfactants including quaternary ammonium, primary amines, and amphoteric cocamidopropyl betaine as the structure-directing agents.[24,26] Strictly speaking, many of the products should be called porous zirconium oxide−sulfate or zirconium oxo phosphates. Their pore sizes are generally less than 4 nm, and their thermal stabilities have been poor. On the basis of the low-angle and high-angle XRD data, preparation of thermally stable mesoporous ZrO_2 with crystalline walls has been claimed;[42] however, from their results, the possibility of phase separation cannot be excluded. Our XRD studies, in combination of bright-field/dark-field TEM
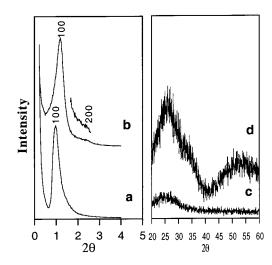
studies represent the first conclusive evidence of thermally stable mesoporous ZrO_2 with a semicrystalline framework.

Niobia. Figure 7 shows typical XRD patterns for mesostructured niobium oxides before and after calcination prepared using $EO_{20}PO_{70}EO_{20}$ as the structure-directing species. The as-synthesized niobium inorganic/polymer mesostructure (Figure 7a) shows a primary diffraction peak with $d = 106$ Å. After calcination, the diffraction peaks appear at higher 2θ angles with $d = 80$ and 41 Å(Figure 7b). These diffraction peaks can be indexed as the (100) and/or (200) reflections from two-dimensional hexagonal mesostructures with lattice constants $a_0 = 122$ and 92 Å, respectively.

The appearance of low-angle X-ray diffraction peaks indicates that mesoscopic order is preserved in the calcined Nb_2O_5 materials, which is confirmed by separate TEM studies. For example, Figure 8a shows a TEM image of mesoporous Nb_2O_5 recorded along the [001] zone axis of the two-dimensional hexagonal mesostructure. The pore/channel walls are continuous and have a mean thickness of ~4 nm. In addition, EDX measurements made on the calcined samples show the expected metal element signal (Figure 8a inset), consistent with the inorganic wall structures being comprised of metal−oxygen networks.

Selected-area electron diffraction patterns recorded on mesoporous Nb_2O_5 show very diffuse electron diffraction rings. Wide-angle X-ray diffraction studies of calcined samples also indicate that the channel walls are essentially amorphous or that nucleation of nanocrystals has perhaps just started at this calcination temperature (400 °C). Bright-field and dark-field TEM imaging did not detect evidence of nanocrystallite formation, unlike mesoporous TiO_2 and ZrO_2.

Figure 8b shows nitrogen sorption isotherms that are representative of mesoporous hexagonal Nb_2O_5. BJH analyses indicate that the calcined hexagonal mesoporous Nb_2O_5 sample possess a mean pore size of 50 Å (Figure 8b inset).[43] Large hysteresis loops that resemble typical H_1-type isotherms are observed for these mesoporous Nb_2O_5 samples, which have surface areas of 196 m^2/g and porosities of 50%.

(41) BdB analysis of hexagonal mesoporous ZrO_2 using cylindrical pore model gives pore size of 55 Å from both the adsorption and desorption isotherms.

(42) Huang, Y.; McCarthy, T. J.; Sachtler, W. M. *Appl. Catal. A* **1996**, *148*, 135.
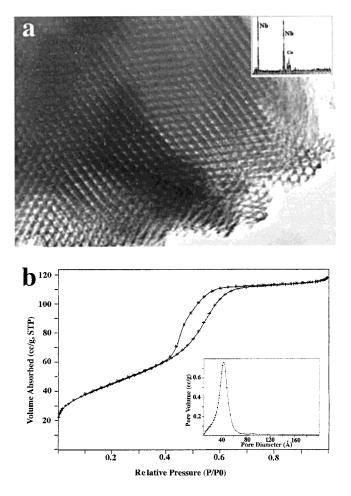
Figure 8. (a) TEM micrograph of two-dimensional hexagonal mesoporous Nb_2O_5 recorded along the [001] zone axis. The corresponding EDX spectrum is shown in the inset. (b) Nitrogen adsorption−desorption isotherms and BJH pore size distribution plot (inset) for calcined Nb_2O_5.

Figure 9. (a) TEM micrograph of two-dimensional hexagonal mesoporous Ta_2O_5 recorded along the [001] zone axis. The corresponding EDX spectrum is shown in the inset. (b) Nitrogen adsorption−desorption isotherms and BJH pore size distribution plot (inset) for calcined Ta_2O_5.

Tantalum Oxide. The as-synthesized tantalum inorganic/polymer mesostructure shows a primary diffraction peak with $d = 110$ Å. After calcination, the diffraction peaks appear at higher 2θ angles with $d = 68$ and 35 Å. These diffraction peaks can be indexed as the (100) and/or (200) reflections from relatively poorly ordered two-dimensional hexagonal mesostructures with lattice constants $a_0 = 127$ and 78 Å, respectively.

The appearance of low-angle diffraction peaks indicates that mesoscopic order is preserved in the calcined Ta_2O_5 materials. This is confirmed by TEM images obtained from mesoporous Ta_2O_5 samples. For example, Figure 9a shows a TEM image of mesoporous Ta_2O_5 recorded along the [001] zone axis of the two-dimensional hexagonal mesostructure. The pore/channel walls are continuous and have a mean thickness of ∼4 nm. In addition, EDX measurements made on the calcined samples show the expected metal element signal (Figure 9a inset), which confirms that the inorganic wall consists of predominantly metal−oxygen networks.

Selected-area electron diffraction patterns recorded on mesoporous Ta_2O_5 show extremely diffuse electron diffraction rings similar to those observed for Nb_2O_5. Wide-angle X-ray diffraction studies of calcined samples also indicate that the channel walls are essentially amorphous or nucleation of nanocrystals at this calcina-
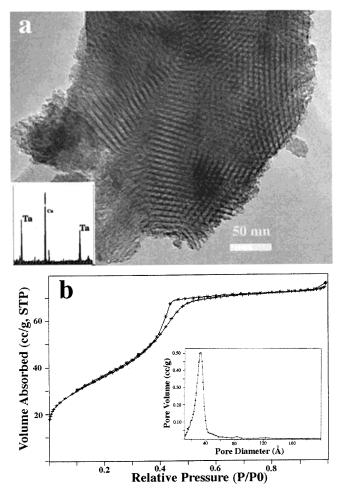
tion temperature (400 °C) has just began. No evidence of nanocrystallite formation is observed in bright-field and dark-field TEM studies.

Figure 9b shows N_2 sorption isotherms that are representative of mesoporous Ta_2O_5. BJH analyses show that the calcined hexagonal mesoporous Ta_2O_5 exhibits mean pore sizes of 35 Å (Figure 9b inset).[44] Hysteresis loops that resemble typical H_1-type isotherms are observed for these mesoporous Ta_2O_5 samples, which have surface areas of 165 m²/g and porosities of 50%.

Tin Oxides. The as-synthesized tin inorganic/polymer mesostructure shows a primary diffraction peak with $d = 124$ Å. After calcination, the diffraction peaks appear at higher 2θ angles with $d = 106$ and 53 Å. These diffraction peaks can be indexed as the (100) and/or (200) reflections from relatively poorly ordered two-dimensional hexagonal mesostructures with lattice constants $a_0 = 143$ and 122 Å, respectively.

Thermogravimetric analyses indicate that the block copolymer species are completely removed from the tin/polymer composite upon calcination at 400 °C. The

(43) BdB analysis of hexagonal mesoporous Nb_2O_5 using cylindrical pore model gives pore size of 45 Å from both the adsorption and desorption isotherms.
(44) BdB analysis of hexagonal mesoporous Ta_2O_5 using cylindrical pore model gives pore size of 35 Å from both the adsorption and desorption isotherms.
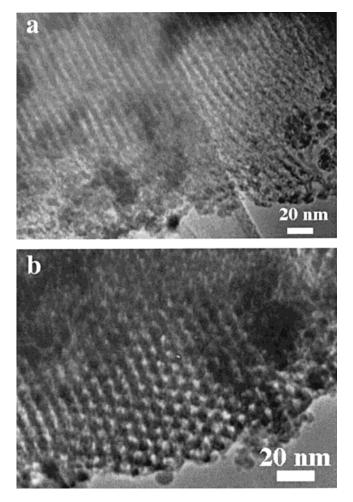
Figure 10. TEM micrographs of two-dimensional hexagonal mesoporous SnO_2 recorded along the [110] (a) and [001] (b) zone axes.

appearance of low-angle diffraction peaks indicates that mesoscopic order is preserved in the calcined SnO_2 materials, which is confirmed by separate TEM measurements. For example, parts a and b of Figure 10 show TEM images of mesoporous SnO_2 recorded along the [ll0] and [001] zone axes of the two-dimensional hexagonal mesostructure. In each case, mesoscopically ordered large channels are clearly observed, with Figure 10b showing their arrangement in hexagonal arrays. The pore/channel walls are continuous and have a mean thickness of ∼5 nm. EDX measurements made on the calcined samples show only metal element signals, which confirm that the framework is predominantly a metal−oxygen network.

Selected-area electron diffraction patterns recorded on mesoporous SnO_2 show characteristic diffuse electron diffraction rings, which indicates that the walls of these materials are made up of nanocrystalline oxides. Wide-angle X-ray diffraction studies of calcined samples also clearly show broad peaks that can be indexed according to the cassiterite crystalline phase. The sizes of the nanocrystals in the calcined materials are estimated to be ∼3 nm by applying the Scherrer formula on the (211) diffraction peak.

Tungsten Oxide. Mesoporous WO_3 was synthesized using $EO_{20}PO_{70}EO_{20}$ as the structure-directing agent. From low-angle XRD measurements, both the as-made tin inorganic/polymer composites and the calcined ox-

ides have two-dimensional hexagonal mesostructures with lattice constants a_0 = 145 and 110 Å, respectively.

Parts a and b of Figure 11 show TEM images of mesoporous WO_3 recorded along the [ll0] and [001] zone axes of the two-dimensional hexagonal mesostructures and reveal ordered large channels arranged in hexagonal arrays. The pore/channel walls are continuous and have a mean thickness of ∼5 nm. Selected-area electron diffraction patterns recorded on mesoporous WO_3 show that the walls of these materials are made up of nanocrystalline oxides that exhibit characteristic diffuse electron diffraction rings. Wide-angle X-ray diffraction studies of calcined samples also clearly show broad peaks that can be indexed according to a crystalline WO_3 phase (JCPDS 20-1324).

EDX analyses (Figure 11c inset) on the calcined samples reveal the expected metal element signals, which confirms that the inorganic wall is comprised predominantly of a metal−oxygen network. Thermogravimetric analyses indicate that the block copolymer species are completely removed from the tungsten/copolymer composite upon calcination at 400 °C (Figure 11d inset). Parts c and d of Figure 11 show nitrogen sorption isotherms that are representative of mesoporous WO_3. BJH analyses show that the calcined hexagonal mesoporous WO_3 sample exhibit mean pore size of 50 Å (Figure 11d).[45] Hysteresis loops that resemble typical H_1-type isotherms are observed for these mesoporous WO_3 samples, which have surface areas of 125 m^2/g and porosities of 48%.

Alumina. Mesoporous alumina was similarly prepared using $EO_{20}PO_{70}EO_{20}$ as the structure-directing agent. TEM images (Figure 12) obtained from mesoporous Al_2O_3 show disordered packed pores with large diameters (10−30 nm).[46] Curved/looped channels (diameter ∼4 nm, not shown) are also observed in these Al_2O_3 samples. Solid-state ^{27}Al magic-angle spinning NMR spectra (not shown) contains signals assigned to primarily six-coordinate Al species in the as-synthesized materials and four-, five-, and six-coordinate Al sites in the calcined products. EDX measurements made on the calcined samples show only Al signal. Selected-area electron diffraction patterns recorded on mesoporous Al_2O_3 indicate that the walls of these materials are essentially amorphous.

Figure 12c shows nitrogen sorption isotherms that are representative of mesoporous Al_2O_3. BJH analyses indicate that the calcined mesoporous Al_2O_3 has a mean pore size of 140 Å (Figure 12c inset).[47] Large hysteresis loops that resemble typical H_1-type isotherms are observed for these mesoporous Al_2O_3 samples. Bimodal pore size distributions are observed for both Al_2O_3 (Figure 12c inset) and SiO_2 samples, which are believed to be due to the coexistence of the different-sized hexagonal packed and curved/looped pore channels.

(45) BdB analysis of hexagonal mesoporous WO_3 using cylindrical pore model gives pore size of 48 Å from both the adsorption and desorption isotherms.

(46) We notice that the ordering lengths and pore sizes of the mesoporous alumina and silica prepared in this study are much larger than other metal oxide system. Exact reasons are not known. One possible reason is the reconstruction of the mesostructure during the calcination for silica and alumina.

(47) BdB analysis of mesoporous Al_2O_3 using cylindrical pore model gives pore size of 120 Å from both the adsorption and desorption isotherms.
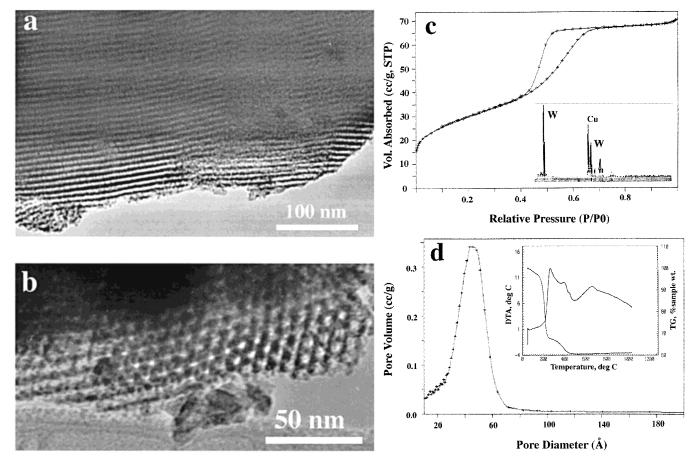
Figure 11. (a and b) TEM micrographs of two-dimensional hexagonal mesoporous WO_3 recorded along the [110] and [001] zone axes. (c and d) Nitrogen adsorption−desorption isotherms and BJH pore size distribution plot for calcined WO_3. Inset in part c is the corresponding EDX spectrum, and in part d the TGA trace obtained on the as-synthesized W(O,Cl)/copolymer composite.
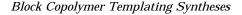
Mixed Oxides. Mesoscopically ordered porous mixed oxides, such as $(SiTi)O_y$ and $(SiAl)O_y$, have also been prepared using similar synthesis procedures. Figure 13 shows typical XRD patterns for mesostructured silicon/titanium oxides before and after calcination prepared using $EO_{20}PO_{70}EO_{20}$ as the structure-directing agent. The as-made Si/Ti inorganic/polymer mesostructure (Figure 13a) shows two diffraction peaks with $d = 103$ and 60 Å. After calcination, the diffraction peaks appear at higher 2θ angles with $d = 95$ and 55 Å (Figure 13b). Both sets of diffraction peaks can be indexed as the (100) and (110) reflections from two-dimensional hexagonal mesostructures with lattice constants of $a_0 = 122$ and 110 Å, respectively.

The low-angle diffraction peaks indicate that mesoscopic order is preserved in the calcined mixed oxide materials. This is confirmed by TEM images obtained from mesoporous $(SiTi)O_y$ samples. For example, parts a and b of Figure 14 show TEM images of mesoporous $(SiTi)O_y$ recorded along the [001] zone axis of the two-dimensional hexagonal mesostructure, in which large ordered channels are clearly observed to be arranged in hexagonal arrays. Parts c and d of Figure 14 show TEM images of mesoporous $(SiAl)O_y$. The pore/channel walls are continuous and have thicknesses of ∼5−7 nm. In addition, EDX measurements made on the calcined samples show the expected metal-only element signals (Figure 15a inset), which confirms that the inorganic wall materials consist of predominantly metal−oxygen networks. The different elements appear to be distrib-

uted uniformly in the amorphous framework within the resolution of EDX measurements.

Figure 15 shows nitrogen sorption isotherms that are representative of mesoporous $SiTiO_y$. BJH analyses show that these calcined mesoporous mixed oxides exhibit pore sizes of 50−100 Å (Figure 15 insets).[48] Similarly, large hysteresis loops that resemble typical H_1-type isotherms are observed for these mesoporous mixed oxides. Table 2 summarizes the d_{100} values measured for the different calcined oxides, along with other physical characteristics and properties. All calcined samples show ordering length scales that are greater than 70 Å.

Thermally Unstable Systems. Among other systems, we have also prepared mesophase of the Mn, Cr, and Cu systems. Optical imaging shows single phase with typical fanlike liquid crystal texture for these systems. Low-angle XRD show reflection peaks up to fourth order (Figure 16a−c), indicating that the materials form well-ordered lamellar mesostructures. The sharp high-angle diffraction peaks (Figure 16d−f) may indicate crystallinity in the layered frameworks. These mesophases, however, are not stable upon calcination and removal of the block copolymer species. Other systems, including Sb, Cd, Zn, In, V, and Re form composite mesophases with $EO_{20}PO_{70}EO_{20}$, based on

---

(48) BdB analysis of hexagonal mesoporous $SiTiO_y$ and Zr_2WO_y using cylindrical pore model gives pore size of 48 and 45 Å from both the adsorption and desorption isotherms.

Block Copolymer Templating Syntheses

Chem. Mater., Vol. 11, No. 10, 1999 **2823**

Figure 13. Low-angle and wide-angle X-ray diffraction (XRD) patterns of (a and c) as-synthesized $(Si,Ti)(O,Cl)/EO_{20}PO_{70}EO_{20}$ composite mesostructure and (b and d) calcined mesoporous $SiTiO_y$.
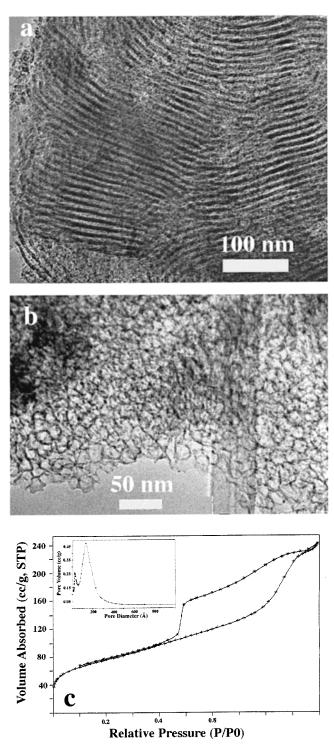
Figure 12. (a and b) TEM micrographs of mesoporous Al_2O_3. (c) Nitrogen adsorption–desorption isotherms and BJH pore size distribution plot (inset) for calcined Al_2O_3.

inorganic–organic interface, thereby disrupting the establishment of mesostructural order.[49,50] This is particularly the case for nonlamellar phases.[50,51] In our approach, undesirable crystallization and macroscopic phase separation are circumvented by using conditions that promote slow hydrolysis of the metal precursors so that self-assembly occurs to produce an amorphous inorganic wall structure. In Figure 1c, for example, the absence of significant high-angle diffraction peaks indicates the walls of the as-made titanium mesostructures are amorphous. This indicates that the large lattice energy associated with the crystallization of the inorganic phases has not interfered with the assembly of the mesophase. During subsequent calcination, the thick walls and noncrystallized inorganic matrix prevent the mesostructures from collapsing, even with nucleation of nanocrystallites, by effectively sustaining the local strain.

The formation of large-pore mesoscopically ordered metal oxides via such a simple and widely applicable procedure suggests that the same general inorganic/block polymer assembly mechanisms may be operating. In fact, it is well-documented that alkylene oxide segments can form crown-ether-type complexes with many inorganic ions through weak coordination bonds.[52] The multivalent metal species (M) can associate preferentially with the hydrophilic PEO moieties, because of their different binding affinities for poly(ethylene oxide) (PEO) and poly(propylene oxide) (PPO). The resulting complexes can then be organized mesoscopically, according to the self-assembly behavior of the hydrophobic/hydrophilic domains of the block copolymer species. The inorganic species subsequently cross-link

their low-angle XRD patterns (Table 1), although they are also not thermally stable. Current efforts in our laboratories are directed toward solving this stability problem by enhancing framework cross-linking in these systems.

Mesophase Formation and Stabilization. Crystallization of inorganic species during the cooperative inorganic/organic self-assembly can lead to macroscopic phase separation of the inorganic and organic components. This is because crystallization energies often dominate the interaction energies that stabilize the
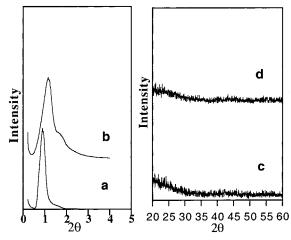
(49) Stucky, G. D.; Belcher, A.; Zaremba, C.; Huo, Q.; Landry, C.; Tolbert, S.; Firouzi, A.; Janicke, M.; Hansma, P.; Morse, D. E.; Chmelka, B. F.; Schacht, S.; Voigt-Martin, I. G.; Schüth, F. *Chemistry on the Nanometer Scale*; The Robert A. Welch Foundation 40th Conference on Chemical Research, Houston, TX; 1996; p 101.

(50) Monnier, A.; Schüth, F.; Huo, Q.; Kumar, D.; Margolese, D.; Maxwell, R. S.; Stucky, G. D.; Krishnamurty, M.; Petroff, P.; Firouzi, A.; Janicke, M.; Chmelka, B. F. *Science* **1993**, *261*, 1299.

(51) Beck, J. S.; Vartuli, J. C.; Roth, W. J.; Leonowicz, M. E.; Kresge, C. T.; Schmitt, K. D.; Chu, C. T. W.; Olson, D. H.; Sheppard, E. W.; MuCullen, S. B.; Higgins, J. B.; Schlenker, J. L. *J. Am. Chem. Soc.* **1992**, *114*, 10834.

(52) Bailey, F. E., Jr.; Koleske, J. V. *Alkylene oxides and their polymers*; Marcel Dekker: New York, 1990.
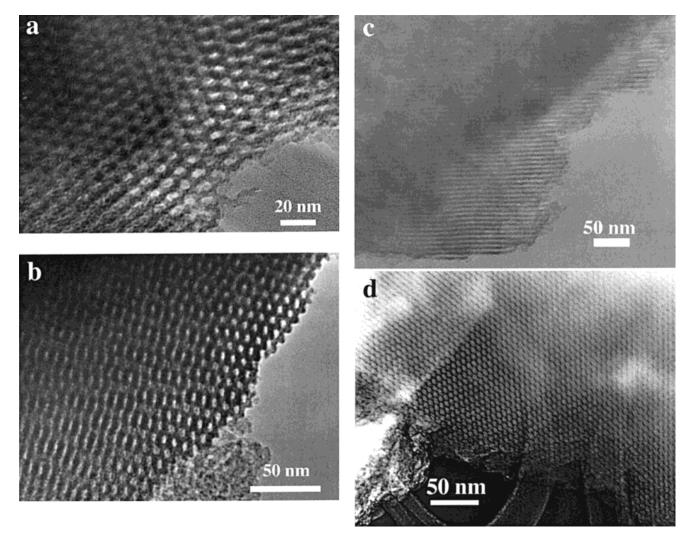
Figure 14. (a and b) TEM micrographs of two-dimensional hexagonal mesoporous $SiTiO_y$ recorded along [001] zone axes. (c and d) TEM micrographs of two-dimensional hexagonal mesoporous $SiAlO_y$ recorded along the [110] and [001] zone axes, respectively.

Table 2. Physicochemical Properties of Mesoporous Metal Oxides Prepared Using $EO_{20}PO_{70}EO_{20}$ as the Structure-Directing Agent[a]

oxide	inorganic precursor	d_{100}[b] (Å)	wall structure	wall thickness[c] (Å)	nanocrystal size[d] (Å)	pore size (Å)	BET surface area (m²/g)	BET surface area (m²/cm³)	porosity[e]	physical properties
ZrO_2	$ZrCl_4$	106	tetra. ZrO_2	65	20	58	150	884	0.43	dielectric
TiO_2	$TiCl_4$	101	anatase	51	30	65	205	867	0.46	semiconductor
Nb_2O_5	$NbCl_5$	80	Nb_2O_5[f]	40	<10	50	196	876	0.50	dielectric
Ta_2O_5	$TaCl_5$	70	Ta_2O_5[f]	40	<10	35	165	1353	0.50	dielectric
WO_3	WCl_6	95	WO_3	50	30	50	125	895	0.48	semiconductor
SnO_2	$SnCl_4$	106	cassiterite	50	30	68	180	1251	0.52	semiconductor
HfO_2	$HfCl_4$	105	amorphous	50	−	70	105	1016	0.52	dielectric
Al_2O_3	$AlCl_3$	186	amorphous	35	−	140	300	1188	0.61	dielectric
SiO_2	$SiCl_4$	198	amorphous	86	−	120	810	1782	0.63	dielectric
$SiAlO_y$	$SiCl_4/AlCl_3$	95	amorphous	38	−	60	310	986	0.59	dielectric
Si_2AlO_y	$SiCl_4/AlCl_3$	124	amorphous	40	−	100	330	965	0.55	dielectric
$SiTiO_y$	$SiCl_4/TiCl_4$	95	amorphous	50	−	50	495	1638	0.63	dielectric
Al_2TiO_y	$AlCl_3/TiCl_4$	105	amorphous	40	−	80	270	1093	0.59	dielectric
$ZrTiO_y$	$ZrCl_4/TiCl_4$	103	amorphous	35	−	80	130	670	0.46	dielectric
ZrW_2O_y	$ZrCl_4/WCl_4$	100	amorphous	45	−	50	170	1144	0.51	NTE[g]

[a] All samples were prepared using ethanol as a solvent, except HfO_2 where butanol was used. [b] d values for samples calcined at 300–600 °C for 5 h in air. [c] Thicknesses measured from TEM experiments. These values are consistent with the values estimated by subtracting the pore diameter from $2d_{100}/\sqrt{3}$. [d] Nanocrystal sizes estimated from X-ray diffraction broadening using the Scherrer formula and the TEM studies. [e] The porosity is estimated from the pore volume determined using the adsorption branch of the N_2 isotherm curve at the $P/P_0 = 0.983$ signal point. [f] Nucleation just started, extremely broad wide-angle diffraction. [g] Materials with negative thermal expansion properties.

and polymerize to form the mesoscopically ordered inorganic/polymer composites, as previously demonstrated also for the assembly of mesostructured silica/

copolymer composites.[14,16] The proposed assembly mechanism for these diverse mesoporous metal oxides uses PEO−metal chelating interactions in conjunction with
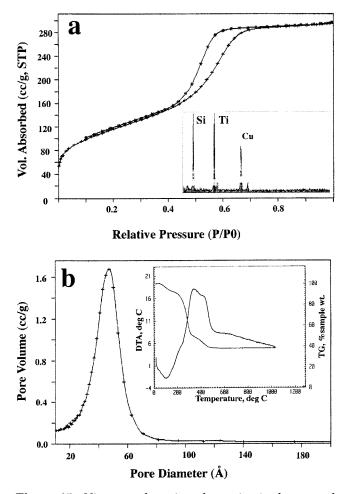
Block Copolymer Templating Syntheses

Chem. Mater., Vol. 11, No. 10, 1999 **2825**

Figure 15. Nitrogen adsorption−desorption isotherms and BJH pore size distribution plot for calcined $SiTiO_y$. Inset in part a is the EDX spectrum taken on the calcined sample; inset in part b is the TGA trace obtained for the as-synthesized sample.
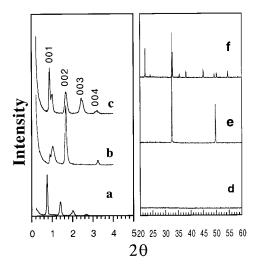

Figure 16. Low-angle and wide-angle X-ray diffraction (XRD) patterns of as-made Cu (O,Cl) (a and d), Mn(O,Cl) (b and e), and Cr(O,Cl) (c and f) /$EO_{20}PO_{70}EO_{20}$ composite mesostructures.

electrostatics, van der Waals forces, etc., to direct meso-structure formation.[3,9,10] The use of interactions between functionalized polymers and inorganic ions for the construction of mesoscopically ordered materials is reminiscent of biomineralization processes in Nature,[53−55]

particularly with regard to amorphous inorganic phases such as amorphous $CaCO_3$.[56]

A novel feature of the current inorganic/copolymer synthesis methodology is using the inorganic precursor in a predominantly nonaqueous media. One advantage of using inorganic salts as precursors is that the rates associated with precursor hydrolysis, condensation of metal species, and precipitation of mesostructured oxides can be performed in a controlled manner.[57,58] Because of the lower electronegativies of the transition metals compared to silicon, their alkoxides undergo nucleophilic reactions such as hydrolysis and condensation more readily. In fact, attempts to synthesize these mesoporous oxides using metal alkoxides as precursors have been mostly unsuccessful in many cases due to their high hydrolysis and/or condensation rates. Considerable work has been directed toward understanding nonhydrolytic sol−gel chemistries of inorganic oxides.[59] Such nonhydrolytic routes involve carbon−oxygen bond cleavage, instead of the metal−oxygen bond and has a general tendency to delay crystallization of the metal oxides. Such deterrence of crystallization appears to be an important prerequisite for the assembly of inorganic−copolymer composite mesostructures. In addition, conventional hydrolytic routes to metal oxides often lead to difficulties in controlling material stoichiometry and homogeneity. Homogeneity depends on the rate of homocondensation (i.e., formation of M−O−M and M′−O−M′) versus the rate of heterocondensation, which is particularly difficult to control in hydrolytic conditions, because of the different reactivities of the various precursors toward hydrolysis and condensation. However, in principle, the nonhydrolytic process should favor the formation of homogeneous binary oxides from different metal precursors, because of decreased differences in the rates of hydrolysis and condensation for different inorganic sources in nonaqueous media. Such nonhydrolytic conditions have been central to our syntheses of mesoporous mixed oxides.

Conclusions

The use of high molecular weight block copolymers as structure-directing agents allows the formation of mesoporous solids with large ordering lengths, thick semicrystalline walls, and large pores. Many amphiphilic block copolymers can be employed to construct mesoporous oxides with tunable ordering lengths and different mesoscopic structures. The ability to synthesize various functional mesoporous oxides demonstrates the versatility of the block copolymer templating approach, which can be used for syntheses of a broader range of nanostructured solids than previously demonstrated. We anticipate that with this method, the syn-

(53) Fritz, M.; Belcher, A. M.; Radmacher, M.; Walters, D. A.; Hansma, P. K.; Stucky, G. D.; Morse, D. E.; Mann, S. *Nature* **1994**, *371*, 49.

(54) Archibald, D. D.; Mann, S. *Nature* **1993**, *364*, 430.

(55) Aksay, I. A.; Trau, M.; Manne, S.; Honma, I.; Yao, N.; Zhou, L.; Fenter, P.; Eisenberger, P. M.; Gruner, S. M. *Science* **1996**, *273*, 892.

(56) Addadi L.; Weiner S. *Nature*, **1997**, *389*, 912; Aizenberg J.; Lambert G.; Addadi L.; Weiner S. *Adv. Mater.* **1996**, *8*, 222.

(57) Livage, J.; Henry, M.; Sanchez, C. *Prog. Solid State Chem.* **1988**, *18*, 259.

(58) Baes, C. F., Jr.; Mesmer, R. E. *The hydrolysis of cations*; John Wiley & Sons: New York, 1976.

(59) Vioux, A. *Chem. Mater.* **1997**, *9*, 2292.

theses of mesoscopically ordered sulfides[33,60] and other mixed oxides should also be possible. Such mesoporous materials, with increasing richness of inorganic compositions and versatile processibilities, have excellent potential for applications as high surface area battery electrodes, sensors, optoelectronic devices, and catalysts.

(60) MacLachlan, M. J.; Coombs, N.; Ozin, G. O. *Nature* **1999**, 397, 681.

Supporting Information Available: Low-angle and high-angle X-ray diffraction patterns for hexagonal mesostructured system of Zr, Ta, and Sn and cubic system of Ti; nitrogen sorption isotherms for mesoporous ZrO_2 and ZrW_2O_y. This material is available free of charge via the Internet at http://pubs.acs.org.

CM990185C